Proc. Natl. Acad. Sci. USA
Vol. 91, pp. 12579–12583, December 1994
Cell Biology

Physiological cytosolic Ca^{2+} transients evoke concurrent mitochondrial depolarizations

(membrane potential/fluorescence/bioenergetics/image processing/microscopy)

LESLIE M. LOEW*†, WALTER CARRINGTON‡, RICHARD A. TUFT‡, AND FREDRIC S. FAY‡

*Department of Physiology, University of Connecticut Health Center, Farmington, CT 06030; and ‡Biomedical Imaging Group, Department of Physiology, University of Massachusetts Medical School, Worcester, MA 01655

Communicated by Britton Chance, August 26, 1994 (received for review May 5, 1994)

ABSTRACT **Calcium, a ubiquitous second messenger, stimulates the activity of several mitochondrial dehydrogenases. This has led to the suggestion that the same messenger that signals cell activation could also activate mitochondrial electron/proton transport, thereby meeting demands for increased cellular energy. To test this in live cells, quantitative three-dimensional microscopy and ratio imaging were used to measure membrane potential of individual mitochondria and cytosolic calcium distribution. Mitochondria reversibly depolarized as cytosolic calcium rose and then fell following physiological stimulation. Thus, the dominant response of the mitochondrion to a rise in cytosolic $[Ca^{2+}]$ is to draw on the electrochemical potential, possibly to accelerate processes directly involved in ATP synthesis and calcium homeostasis.**

The electrochemical potential difference across the inner mitochondrial membrane that drives ATP synthesis (1, 2) has two components: the largest component is an electrical potential difference of *ca.* −150 mV; the remainder is due to a pH gradient corresponding to *ca.* 1 pH unit (equivalent to −60 mV). The electrical component provides a large driving force for the entry of divalent cations, making mitochondria an excellent intracellular sink that the cell may utilize to overcome sudden calcium loads or turn off a calcium signal once it has sufficiently activated its cytoplasmic targets. Indeed, *in vitro* studies on mitochondrial suspensions have shown that they can help to counter large Ca^{2+} loads, approaching cytotoxic levels, where mitochondrial calcium efflux pathways are saturated (3–5). Thus, when challenged with sufficiently high $[Ca^{2+}]$, the mitochondria can contribute to cytosolic calcium homeostasis.

Recently, however, elegant experiments on mitochondria in single living cells have shown that even physiological cytosolic $[Ca^{2+}]$ ($[Ca^{2+}]_{cyt}$) increases are also accompanied by mitochondrial Ca^{2+} uptake (6–8). The significance of this Ca^{2+} uptake for cellular or mitochondrial function has not been determined, but one idea is that mitochondrial respiration may be stimulated by the observed increase in $[Ca^{2+}]$. Support for this suggestion is based on the finding that dehydrogenase activity is potentiated at high Ca^{2+} (9–11) and that direct measurement in a single cell reveals that a rise in calcium induces an increase in oxidative metabolism (12). Thus, an increased mitochondrial $[Ca^{2+}]$ could, via the dehydrogenase pathway, increase the electrochemical gradient and thereby enhance ATP synthesis. Alternatively, calcium influx into mitochondria could also lead to a direct dissipation of the electrical component of the electrochemical gradient or activate the ATP synthase that uses the energy stored in the gradient (13). It is important, therefore, to determine the effect of physiological calcium signals on the mitochondrial electrochemical potential *in situ*.

The publication costs of this article were defrayed in part by page charge payment. This article must therefore be hereby marked "*advertisement*" in accordance with 18 U.S.C. §1734 solely to indicate this fact.

Fluorescent probes have been primary tools in studies of mitochondrial physiology and have helped to substantiate the chemiosmotic theory. This is because direct electrophysiological recordings are not possible with an organelle as small and complex as the mitochondrion. Potentiometric dyes, primarily of the oxonol (14, 15) and cyanine (16) classes, have been developed to determine the electrical potential across the inner mitochondrial membrane in isolated mitochondrial suspensions (17). For investigations in single cells, cationic dyes of the cyanine, styryl, and rhodamine classes display potential-dependent accumulations inside mitochondria, permitting qualitative estimations of changes in membrane potential by fluorescence microscopy (18–20). None of these approaches permits the quantitative determination of possibly small calcium-dependent changes in the membrane potential of mitochondria inside intact cells.

We have recently developed a method for measuring the electrical potential difference across the membrane of individual mitochondria inside a living cell (21). The approach is based on applying the Nernst equation to the distribution of a fluorescent membrane-permeant cationic dye between the mitochondrial and cytosolic compartments. This idea had previously been applied to measuring the potential across the plasma membrane (22–24), but the application to mitochondria proved to be a challenge. Primarily, this is because the fluorescence from the small volume of a single mitochondrion is diluted by the lower fluorescence of the dye emanating from above and below the mitochondrion within the depth of focus of the microscope. Indeed, even confocal microscopy cannot solve this problem because the confocal "optical slice" is still several times thicker than the diameter of most mitochondria (23, 25). We solved this problem by processing three-dimensional (3D) widefield microscope fluorescence images with a constrained iterative deconvolution algorithm (26, 27) and further correcting the data with the results of model calculations (21). In this paper, we combine this method with cytosolic calcium imaging (28, 29) to determine, *in situ*, how physiological $[Ca^{2+}]_{cyt}$ increases affect the electrical component of the mitochondrial electrochemical potential.

METHODS AND MATERIALS

Differentiated N1E-115 neuroblastoma cells were grown on no. 1 coverslips according to published procedures (30). Cells were loaded with fura-2 as described (31). A coverslip was mounted on a microscope chamber thermostatted to 37°C and equilibrated with 100 nM tetramethylrhodamine ethyl ester perchlorate (TMRE) (22) in a balanced salt solution containing 10 mM glucose.

Abbreviations: TMRE, tetramethylrhodamine ethyl ester perchlorate; $[Ca^{2+}]_{cyt}$, cytosolic $[Ca^{2+}]$; CCD, charge-coupled device; 3D, three-dimensional; V_{mit}, mitochondrial membrane potential.

†To whom reprint requests should be addressed.

The 3D microscope utilized for these studies was based on a previously described design (21) with the addition of a second illumination system for dual-wavelength fura-2 excitation; the key features of this apparatus are depicted in Fig. 1. Widefield fura-2 images are taken at a single focal position ($z = 0$) with 0.5- or 1-s arc lamp exposures through 340-nm and 380-nm fura excitation filters. Time between these two excitation exposures is no longer than ≈0.2 s, the filter wheel rotation time, the 2-ms parallel charge transport time for 73 lines being negligible. The two strip images on the charge-coupled device (CCD) are then read out in 1.7 s, during which time DM2 is moved to the TMRE position. A series of seven 5-ms laser exposures are taken at $z = -1.2, -0.6, -0.3, 0, 0.3, 0.6$, and 1.2 μm, with 20 ms between exposures to allow for relaxation of the deformations introduced in the chamber coverslip by coupling of the objective motion through the glycerin immersion medium. The resulting seven image through-focus series is read out in ≈6 s.

Images obtained at the central focal plane at 340- and 380-nm excitation, 500-nm emission were used to calculate (28) an image of $[Ca^{2+}]$. Images of TMRE fluorescence at 514-nm excitation, 550-nm emission were obtained at seven focal planes and processed utilizing a constrained deconvolution algorithm to move out-of-focus light in the set of images to its point of origin. The mitochondrial fluorescence was further corrected with a model-based calibration of the restoration accuracy. The ratio of fluorescence intensity at the most in-focus, brightest, point in each mitochondrion to that in the neighboring cytosol was used to calculate the membrane potential of that mitochondrion; full details of these methods have been published (21).

TMRE was prepared according to the procedure detailed by Ehrenberg *et al.* (22) but is also commercially available (Molecular Probes). Fura-2 AM was obtained from Molecular Probes, bradykinin was from Sigma, and ionomycin free acid was from Calbiochem.

RESULTS

To assess for possible effects of $[Ca^{2+}]_{cyt}$ on mitochondrial electrochemical potential, images of both $[Ca^{2+}]_{cyt}$ and membrane potential of individual mitochondria (V_{mit}) were obtained in single living N1E-115 neuroblastoma cells during their response to stimulation. $[Ca^{2+}]_{cyt}$ changes in these cells can be elicited via both activation of voltage-sensitive calcium channels (31–34) and release of calcium from intracellular stores (35), permitting us to measure the response of V_{mit} to either source of physiological calcium signal. Measurements of $[Ca^{2+}]_{cyt}$ were obtained with the ratiometric indicator fura-2 (28) and V_{mit} with the membrane-permeant cationic dye TMRE (22). We have previously shown that this dye neither binds appreciably to cell membranes nor self

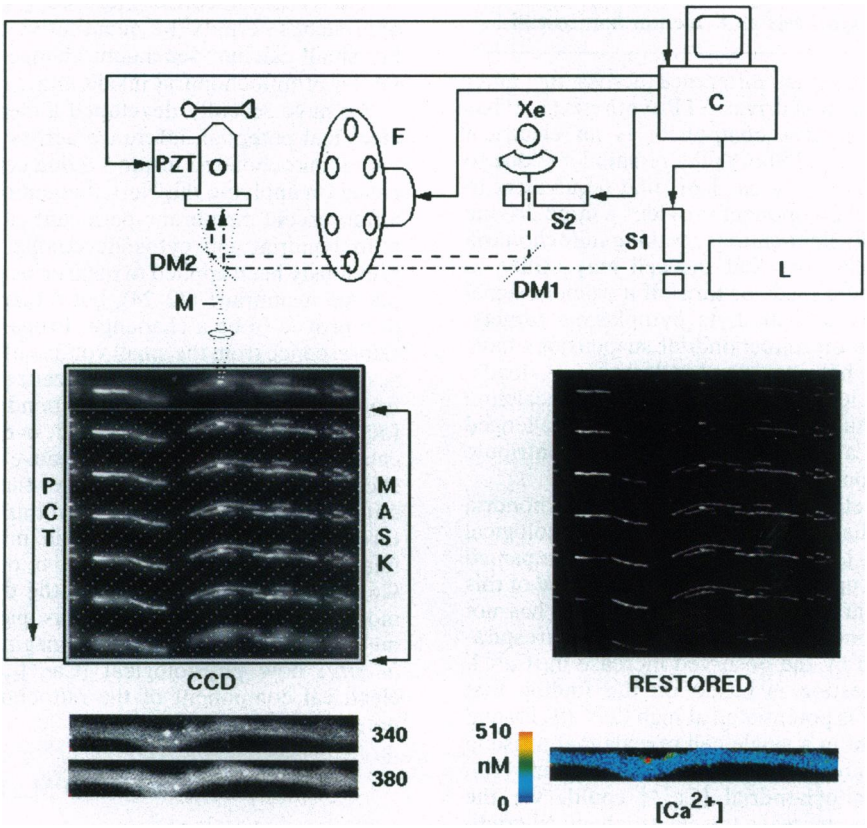

FIG. 1. Fast quantitative microscopy scheme to measure the mitochondrial membrane potential (V_{mit}) with TMRE and $[Ca^{2+}]_{cyt}$ with fura-2. The argon-krypton laser (L) (Coherent, Palo Alto, CA), run typically at 100 mW at 514 nm, is beam expanded and directed to the epi-illumination optics of a custom-built inverted microscope, providing a widefield illumination flux of $\approx 1 \times 10^{21}$ photons $cm^{-2}s^{-1}$ at the specimen plane. S1 and S2, shutters (Uniblitz, Rochester, NY). Xe, 75-W xenon arc lamp (Osram) in Zeiss housing with quartz collector. DM1, dichroic mirror, 400-nm long-pass. F, motorized filter wheel (MVI, Avon, MA). O, objective, Nikon 100× UV-F numerical aperture 1.3 glycerin. PZT, piezoelectric translator, 20-μm total travel (Polytec Optronics, Costa Mesa, CA). DM2, two-position epi-illumination dichroic mirror and emission filter cube: position 1, 400-nm long-pass dichroic and 500-nm long-pass emission filter for fura-2; position 2, 530-nm long-pass dichroic and 550-nm long-pass emission filter for TMRE. M, mask in intermediate image plane limits image area relayed to camera. CCD, CCD camera (Photometrics, Tucson, AZ) with Tektronix TK512 thinned, back-illuminated CCD; images are formed on a 73 × 512 pixel strip defined by mask M, the remaining area being used to store previous strip images. PCT, parallel charge transport, the means by which each strip image is moved under the masked area of the CCD during the time between exposures. C, system and camera controller. The images show the fluorescence distribution in a process from a live neuroblastoma cell loaded with fura-2 and in the presence of TMRE.

quenches over the concentration range required to assess V_{mit} (21–23). Thus, fluorescence intensity is proportional to concentration, and the ratio of dye brightness inside the mitochondrion relative to that in the surrounding cytosol provides an estimate of the membrane potential of individual mitochondria via the Nernst equation (21). As illustrated in Fig. 1, the requisite high-resolution measurements of TMRE fluorescence intensity were obtained from a series of images taken at seven focal planes with a novel microscope that acquired these images at such high speeds that there is negligible displacement of the rapidly locomoting mitochondria during acquisition of the 3D data. As a consequence, these data can be processed with a calibrated constrained iterative deconvolution algorithm (26, 27) utilizing an empirically determined point spread function to reassign out-of-focus light in the series of images to the proper 3D position. These restored images of TMRE fluorescence and a pair of fura-2 fluorescence images taken at 340- and 380-nm excitation were used to estimate V_{mit} in individual mitochondria and $[Ca^{2+}]_{cyt}$ in the neurites of these cells, respectively.

Fig. 2 shows the results of an experiment in which a cell is depolarized with elevated extracellular potassium. $[Ca^{2+}]_{cyt}$ rises from a prestimulus level of 98 nM to a mean of 188 nM 30 s after introduction of 135 mM K^+; this is accompanied by a 10-mV depolarization of the mean V_{mit} from its original level of −157 mV. In this experiment, the $[Ca^{2+}]_{cyt}$ rise is not uniform, being higher on the right side of the cell; this may be due to an uneven distribution of calcium channels in the plasma membrane (34, 36). Although the number of mitochondria in this imaged portion of the cell is too small to establish a statistically significant correlation, it is striking that the pattern of V_{mit} generally parallels the $[Ca^{2+}]_{cyt}$ distribution. The reversibility of the response is demonstrated at the bottom of Fig. 2, which shows that the $[Ca^{2+}]_{cyt}$ recovers to prestimulus levels following reintroduction of normal low K^+ solution as does V_{mit}. The reversibility of the response demonstrates that the multiple light exposures do not lead to significant phototoxic damage. Control experiments with no stimulation generally showed the $[Ca^{2+}]_{cyt}$ and V_{mit} to be stable during up to four complete cycles of 340/380 nm and seven laser exposures used to excite the fluorescence of the indicators, but in some cells mitochondrial depolarizations (accompanied by significant swelling) were observed. Experiments were run with minimal light intensities and exposure times, consistent with acceptable data precision, but the problem of phototoxicity limited our ability to follow changes over longer periods or with higher temporal resolution.

Results similar to those in Fig. 2 were observed in nine other cells exposed to high potassium. In this group of cells, $[Ca^{2+}]_{cyt}$ increased from an average resting level of 104 ± 16 (SE) nM to a poststimulus mean level of 256 ± 33 nM. This was accompanied by a depolarization of the average V_{mit} from −146 ± 3 mV to −132 ± 3 mV; all nine of these cells showed both $[Ca^{2+}]_{cyt}$ rises and V_{mit} depolarizations. The change in V_{mit} in this series was highly significant ($P < 0.001$, by paired t test). In seven of these experiments, we allowed the cells to recover for 5 min following removal of the high K^+ stimulus; all seven showed recoveries toward the prestimulus levels of both $[Ca^{2+}]_{cyt}$, averaging 112 ± 17 nM, and V_{mit}, averaging −141 ± 4 mV; the V_{mit} recovery in each experiment was highly significant ($P < 0.005$, by paired t test). The fact that V_{mit} recovers provides reassurance that the depolarization is not due to artifactual fluorescence bleaching or photodynamic damage.

The effect of bradykinin, which evokes a transient $[Ca^{2+}]_{cyt}$ rise due to calcium release from intracellular stores (35), is shown in Fig. 3. The histograms of V_{mit} distribution before (Fig. 3*a*) and immediately after (Fig. 3*b*) treatment with 250 nM bradykinin reveal that a $[Ca^{2+}]_{cyt}$ rise in response to this stimulus is accompanied by mitochondrial depolarizations. Interestingly, the distribution of V_{mit} is broadened with several individual mitochondria displaying especially depolarized potentials. Such broadened and/or skewed distributions of V_{mit} were noted in cells stimulated by high $[K^+]$ or bradykinin. There was no apparent $[Ca^{2+}]_{cyt}$ nonuniformity in this cell, however. In Fig. 3*c*, $[Ca^{2+}]_{cyt}$ and V_{mit} are shown to recover to near prestimulus levels after several minutes, even in the continued presence of the drug. In seven such experiments, the average initial rise in $[Ca^{2+}]_{cyt}$ was 159 ± 29 nM and the average depolarization of V_{mit} was 15 ± 4 mV ($P < 0.02$ by paired t test); both of these changes are comparable to the average changes evoked by the K^+ depolarization experiments. Initial rises in $[Ca^{2+}]_{cyt}$ and depolarizations of V_{mit} were observed in all seven of these experiments. In six of these experiments, dual-wavelength fura-2 and 3D TMRE images were acquired after *ca.* 5 min of

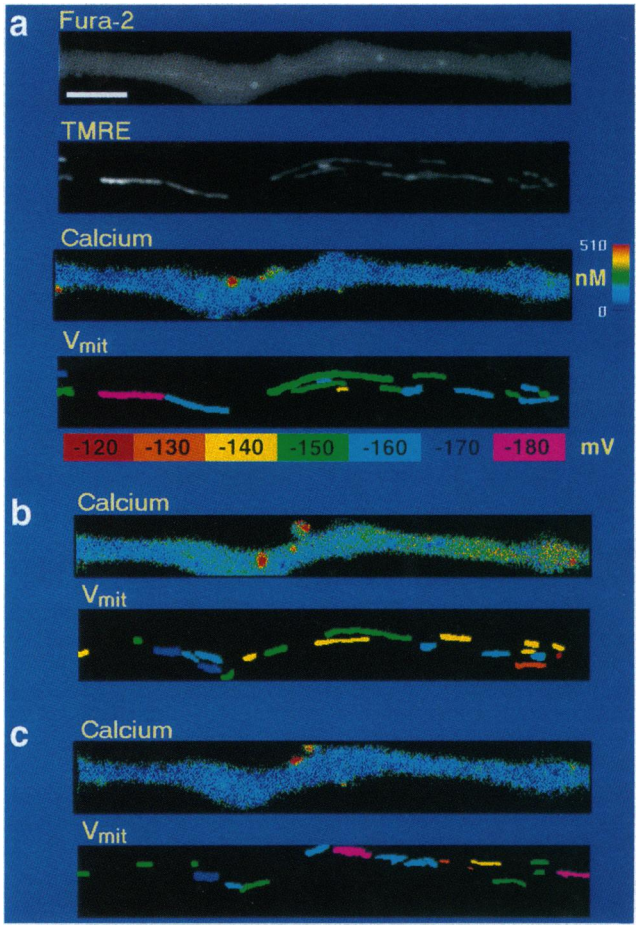

FIG. 2. Potassium evokes a $[Ca^{2+}]_{cyt}$ rise and V_{mit} depolarization. (*a*) The top panel is a prestimulus image of a neurite loaded with fura-2 and shown with 380-nm excitation. The image labeled TMRE is a projection of a restored 3D image of the same cell showing the distribution of TMRE fluorescence in mitochondria. The color-mapped calcium image of the same cell shows a uniform $[Ca^{2+}]_{cyt}$ of 98 nM. Analysis of the restored 3D TMRE image (21) permits calculation of V_{mit} for each fully segmentable mitochondrion; the potentials were color coded in 10-mV steps as shown at the bottom. (*b*) Calcium and V_{mit} distributions 30 s after treatment of the same cell with 135 mM K^+. The $[Ca^{2+}]_{cyt}$ is elevated overall but also displays a gradient from *ca.* 120–300 nM left to right. The average V_{mit} is depolarized by 10 mV but a gradient is also apparent showing the greatest depolarization on the right—i.e., in the same region as the highest $[Ca^{2+}]_{cyt}$. (*c*) The same cell was returned to normal $[K^+]$ and after 5 min the calcium is back to a uniform 102 nM. The V_{mit} now once again displays a random spatial distribution and the mean has recovered to within 3 mV of the prestimulus mean in *a*.

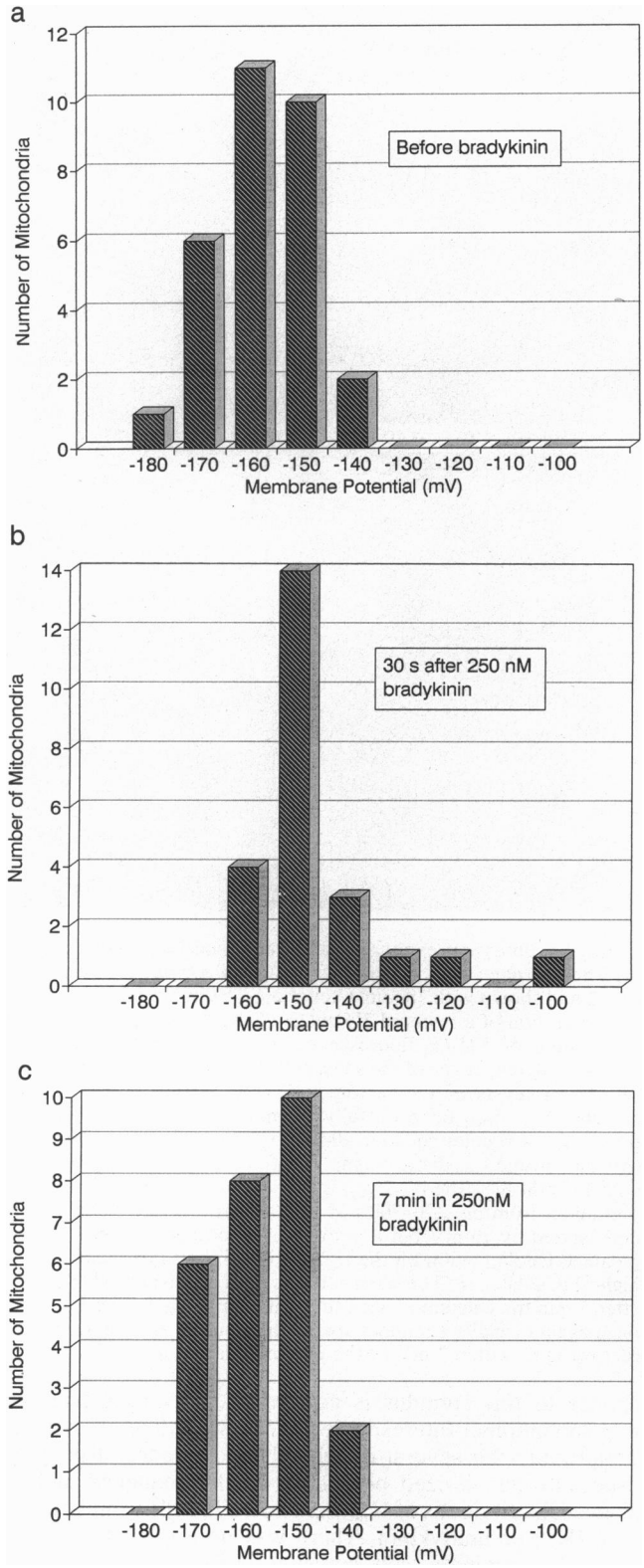

FIG. 3. Bradykinin evokes a transient $[Ca^{2+}]_{cyt}$ rise and a transient V_{mit} depolarization. (*a*) Histogram of V_{mit} distribution in a neurite prior to treatment. $<[Ca^{2+}]_{cyt}> = 56$ nM, $<V_{mit}> = 158$ mV. (*b*) The same cell analyzed 30 s after treatment with 250 nM bradykinin; $<[Ca^{2+}]_{cyt}> = 210$ nM, $<V_{mit}> = 147$ mV; the histogram shows an abnormal distribution with several highly depolarized mitochondria. (*c*) After 4 min in the presence of bradykinin, the $<[Ca^{2+}]_{cyt}>$ has recovered to 96 nM and the $<V_{mit}>$ to 157 mV.

exposure to bradykinin (Fig. 3*c* is an example). In all of these, the $[Ca^{2+}]_{cyt}$ had recovered to near prestimulus levels (averaging 120 ± 16 nM after 5 min with bradykinin vs. 97 ± 12 nM before bradykinin addition). A recovery of V_{mit} was observed in five of these six cells. The mean V_{mit} was 150 ± 5 mV vs. a pretreatment average of 155 ± 5 mV; the recovery was again highly significant ($P < 0.005$, paired *t* test). One cell showed an increased average depolarization of the mitochondria at this later time point amounting to 30 mV. This aberrant result may be due to phototoxic effects on the mitochondria.

DISCUSSION

In view of the recent studies indicating that physiological changes in $[Ca^{2+}]_{cyt}$ evoke parallel changes in $[Ca^{2+}]_{mit}$ (6–8), we believe that the depolarizations of V_{mit} described in this report may be most easily understood in terms of a direct effect of calcium, rather than some other, as yet unidentified, cytosolic messenger. This conclusion is supported by the ability of V_{mit} to mirror both increases and decreases in $[Ca^{2+}]_{cyt}$, irrespective of whether they are initiated by opening of voltage-sensitive Ca^{2+} channels in the plasma membrane or by release of Ca^{2+} from intracellular stores.

The finding that mitochondrial dehydrogenases are activated by calcium (9–11) has led to the suggestion that increases in $[Ca^{2+}]_{cyt}$ would be expected to cause an increased V_{mit} (and ΔpH) leading to enhanced ATP synthesis. The results presented in this report do not support the prediction that increased $[Ca^{2+}]_{cyt}$ should cause mitochondrial hyperpolarization in an intact living cell. How might the observed changes in V_{mit} be linked to $[Ca^{2+}]_{cyt}$? For one, it is possible that the influx of Ca^{2+} into the mitochondria is directly responsible for the observed depolarization. Generally, the flux expected from the increases in $[Ca^{2+}]_{cyt}$ reported here would not be expected to be competitive with the proton pumping rates that sustain V_{mit} (4). However, the possibility of calcium release sites immediately adjacent to mitochondria, exposing them to high local $[Ca^{2+}]$, has been suggested by the intramitochondrial calcium measurements of Pozzan and his colleagues (8). These associations could be heterogeneously distributed and could explain the skewed distributions of depolarized mitochondria during a $[Ca^{2+}]_{cyt}$ rise (Fig. 3).

An alternative explanation for the observed mitochondrial depolarization in association with a rise in $[Ca^{2+}]_{cyt}$ is that activation of the cell by either of the stimuli employed here could be placing a stress on the cell's energy stores, driving down the ATP/ADP ratio; this, in turn, would drive ATP synthesis and run down the electrochemical gradient (37, 38). It is unlikely that such changes would produce such a rapid response, however. We have found (21) that the cell retains the capacity to drive energy-dependent processes for up to 20 min after the mitochondria are completely poisoned with an uncoupler, suggesting that cellular energy stores are well buffered over the time interval of the observed changes. Finally, calcium has also been shown to affect the activity of the ATP synthase (13, 37) and this could drive down the mitochondrial electrochemical potential. Indeed, a recent elegant study on living heart showed that increasing load resulted in a decreased V_{mit} (39) without an increased concentration of ADP but with an increased rate of oxygen consumption. Thus, increased activity, with its accompanying calcium signal, is likely to increase Ca^{2+} uptake into mitochondria, ATP synthesis, and electron transport. Our study indicates that the change in mitochondrial membrane potential effected by $[Ca^{2+}]_{cyt}$ increases is dominated, at least in this neuronal cell line, by Ca^{2+} uptake and/or the stimulation of ATP synthesis, rather than enhanced electron transport.

We are indebted to Kevin Fogarty and Doug Bowman for providing the image analysis software and for their invaluable technical

advice. Technical assistance was graciously provided by Kristine Perry and Mei-de Wei. Generous access to the Silicon Graphics, Inc., Power Series computer was provided by John Carson and Frank Morgan. The financial support of the National Institute for General Medical Sciences (GM35063) and the National Science Foundation (BIR-9200027) is gratefully acknowledged.

1. Mitchell, P. (1961) *Nature (London)* **191,** 144–148.
2. Chance, B., Boyer, P. B., Ernster, L., Mitchell, P., Racker, E. & Slater, E. C. (1977) *Annu. Rev. Biochem.* **46,** 955–1026.
3. Carafoli, E. (1987) *Annu. Rev. Biochem.* **56,** 395–433.
4. Gunter, T. E. & Pfeiffer, D. R. (1990) *Am. J. Physiol.* **258,** C755–C786.
5. Crompton, M. (1990) in *Intracellular Calcium Regulation*, ed. Bronner, F. (Liss, New York), pp. 181–209.
6. Miyata, H., Silverman, H. S., Sollott, S. J., Lakatta, E. G., Stern, M. D. & Hansford, R. G. (1991) *Am. J. Physiol.* **261,** H1123–H1134.
7. Rizzuto, R., Simpson, A. W. M., Brini, M. & Pozzan, T. (1992) *Nature (London)* **358,** 325–327.
8. Rizzuto, R., Brini, M., Murgia, M. & Pozzan, T. (1993) *Science* **262,** 744–747.
9. Hansford, R. G. (1985) *Rev. Physiol. Biochem. Pharmacol.* **102,** 1–72.
10. McCormack, J. G. & Denton, R. M. (1986) *Trends Biochem. Sci.* **11,** 258–262.
11. McCormack, J. G., Halestrap, A. P. & Denton, R. M. (1990) *Physiol. Rev.* **70,** 391–425.
12. Fein, A. & Tsacopoulos, M. (1988) *Nature (London)* **331,** 437–441.
13. Harris, D. A. & Das, A. N. (1991) *Biochem. J.* **280,** 561–573.
14. Chance, B. (1975) in *Biochemistry Series: Energy Transducing Mechanisms*, ed. Racker, E. (Butterworth, London), pp. 1–29.
15. Smith, J. C., Russ, P., Cooperman, B. S. & Chance, B. (1976) *Biochemistry* **15,** 5094–5105.
16. Laris, P. C., Bahr, D. P. & Chaffee, R. R. J. (1975) *Biochim. Biophys. Acta* **376,** 415–425.
17. Smith, J. C. (1988) in *Spectroscopic Membrane Probes*, ed. Loew, L. M. (CRC, Boca Raton, FL), Vol. 2, pp. 153–191.
18. Johnson, L. V., Walsh, M. L., Bockus, B. J. & Chen, L. B. (1981) *J. Cell Biol.* **88,** 526–535.
19. Chen, L. B. (1988) *Annu. Rev. Cell Biol.* **4,** 155–181.
20. Smiley, S. T., Reers, M., Mottola-Hartshorn, C., Lin, M., Chen, A., Smith, T. W., Steele, G. D. & Chen, L. B. (1991) *Proc. Natl. Acad. Sci. USA* **88,** 3671–3675.
21. Loew, L. M., Tuft, R. A., Carrington, W. & Fay, F. S. (1993) *Biophys. J.* **65,** 2396–2407.
22. Ehrenberg, B., Montana, V., Wei, M.-d, Wuskell, J. P. & Loew, L. M. (1988) *Biophys. J.* **53,** 785–794.
23. Farkas, D. L., Wei, M., Febbroriello, P., Carson, J. H. & Loew, L. M. (1989) *Biophys. J.* **56,** 1053–1069.
24. Loew, L. M. (1993) in *Methods in Cell Biology, 38: Cell Biological Applications of Confocal Microscopy; Methods in Cell Biology*, ed. Matsumoto, B. (Academic, Orlando, FL), Vol. 38, pp. 194–209.
25. Chacon, E., Reece, J. M., Nieminen, A.-L., Zahrebelski, G., Herman, B. & Lemasters, J. J. (1994) *Biophys. J.* **66,** 942–952.
26. Carrington, W. A. (1990) in *Proceedings on Bioimaging and Two Dimensional Spectroscopy*, ed. Smith, L. C. (SPIE, Los Angeles), pp. 72–83.
27. Carrington, W., Fogarty, K. E. & Fay, F. S. (1990) in *Non-Invasive Techniques in Cell Biology*, ed. Foster, K. (Wiley, New York), pp. 53–72.
28. Grynkiewicz, G., Poenie, M. & Tsien, R. Y. (1985) *J. Biol. Chem.* **260,** 3440–3450.
29. Tsien, R. Y. & Poenie, M. (1986) *Trends Biochem. Sci.* **11,** 450–455.
30. Kimhi, Y., Palfrey, C., Spector, I., Barak, Y. & Littauer, U. (1976) *Proc. Natl. Acad. Sci. USA* **73,** 462–466.
31. Bedlack, R. S., Wei, M.-d & Loew, L. M. (1992) *Neuron* **9,** 393–403.
32. Moolenaar, W. H. & Spector, I. (1977) *Science* **196,** 331–332.
33. Moolenar, W. & Spector, I. (1979) *J. Physiol. (London)* **292,** 297–306.
34. Bolsover, S. & Spector, I. (1986) *J. Neurosci.* **6,** 1934–1940.
35. Monck, J. R., Williamson, R. E., Rogulja, I., Fluharty, S. J. & Williamson, J. R. (1990) *J. Neurochem.* **54,** 278–287.
36. Silver, R. A., Lamb, A. G. & Bolsover, S. R. (1990) *Nature (London)* **343,** 751–754.
37. Brown, G. C. (1992) *Biochem. J.* **284,** 1–13.
38. Brand, M. D. & Murphy, M. P. (1987) *Proc. Cambridge Philos. Soc.* **62,** 141–193.
39. Wan, B., Doumen, C., Duszynski, J., Salama, G., Vary, T. C. & LaNoue, K. (1993) *Am. J. Physiol.* **265,** H453–H460.